
The GEOsensor Project: Rotations – a New Observable for Seismology

U. Schreiber¹, H. Igel², A. Cochard², A. Velikoseltsev¹, A. Flaws³,
B. Schuberth², W. Drewitz⁴ and F. Müller⁴

¹ Forschungseinrichtung Satellitengeodäsie der TU- München
schreiber@wettzell.ifag.de, alex@wettzell.ifag.de

² Department für Geo- und Umweltwissenschaften, Sektion Geophysik,
Ludwig-Maximilians-Universität München
igel@geophysik.uni-muenchen.de, alain@geophysik.uni-muenchen.de

³ Department of Physics and Astronomy, University of Canterbury, New Zealand
acf28@student.canterbury.ac.nz

⁴ FMB Feinwerk- und Messtechnik GmbH, Berlin
w.drewitz@fmb-berlin.de f.mueller@fmb-berlin.de

Summary. Over the last 40 years ring laser gyroscopes became one of the most important instruments in the field of inertial navigation and precise rotation measurements. They have a high resolution for angular velocities, a very good scale factor stability and a wide dynamic range. These properties made them suitable for aircraft and autonomous submarine navigation. Over the last decade we have developed several very large perimeter ring laser gyroscopes for the application in geodesy and geophysics (Schreiber et al., 2001). Because of a substantial upscaling of these ring lasers, their sensitivity to rotations has been increased by at least 5 orders of magnitudes. At the same time the instrumental drift was reduced by about the same amount. This progress in rotational sensor technology led to the successful detection of rotational signals caused by earthquakes (Pancha et al., 2000) several thousands kilometers away. These observations stimulated the development of a highly sensitive ring laser gyro for specific seismological applications. The GEOsensor provides rotational motions along with the usual translational motions at a high data acquisition rate of at least 20 Hz. Observations of seismic induced rotations show that they are consistent in phase and amplitude with the collocated recordings of transverse accelerations obtained from a standard seismometer over a wide range of distances and frequencies.

Key words: ring laser, seismology, rotation measurements

1 Introduction

Currently there are primarily two types of measurements that are routinely used to monitor global and regional seismic wave fields. Standard inertial seis-

ometers measure three components of translational ground displacement and provide the basis for monitoring seismic activity and ground motion. The second type aims at measuring the deformation of the Earth (strains). It is well known (Aki and Richards, 2002) that there is a third type of measurement that should be observed in seismology and geodesy in order to fully describe the motion at a given point, the measurement of ground rotation. In the past years, ring laser gyroscopes were developed primarily to observe variations in Earth's absolute rotation rate with high precision (Stedman et al., 1995; Stedman, 1997). The recording of the (complete) earthquake-induced rotational motion is expected to be useful particularly for (1) further constraining earthquake source processes when observed close to the active faults (Takeo and Ito, 1997); (2) estimating permanent displacement from seismic recordings (Trifunac and Todorovska, 2001); (3) estimating local (horizontal) phase velocities from collocated observations of translations and rotations (Igel et al., 2005a).

In standard analysis approaches in seismology earthquake induced rotations have been neglected in the past, because the corresponding magnitudes were thought to be small and no suitable instruments with the required resolution existed. The high sensitivity for rotations of large ring lasers along with their insusceptibility to linear translations makes the application of these instruments very attractive for seismological studies. The required range of angular velocities to be measured is expected to be 10^{-14} rad/s Ω_s 1 rad/s and the required frequency bandwidth for the seismic waves is in the range of 3 mHz f_s 10 Hz (Schreiber et al., 2004). Three such devices mounted in orthogonal orientations will eventually provide the quantitative detection of rotations from shear, Love and Rayleigh waves, thus providing the missing quantities for a complete 6 degrees of freedom measurement system.

2 Instrumental Section

Ring lasers are active Sagnac interferometers, where two laser beams are circulating around a triangular or square closed cavity in opposite directions (Aronowitz, 1971). If the whole apparatus is rotating with respect to inertial space one obtains a frequency splitting of the two counter propagating waves, which is proportional to the rate of rotations. The Sagnac frequency δf is

$$\delta f = \frac{4A}{\lambda P} \mathbf{n} \cdot \boldsymbol{\Omega} , \quad (1)$$

where A is the area, P the perimeter enclosed by the beam path and λ the optical wave length of the laser oscillation. $\boldsymbol{\Omega}$ is the angular velocity at which the instrument is turning and \mathbf{n} is the normal vector to the laser beam plane. The resolution of a ring laser gyroscope is proportional to the ratio of the quotient of area and perimeter enclosed by the beam path. Therefore, an increased size of the laser cavity leads to an improved sensor sensitivity. For example, the

4 by 4 meters square ring laser G installed in Fundamentalstation Wettzell (Germany) has a sensor resolution of $\delta\varphi = 9 \cdot 10^{-11} \text{rad}/\sqrt{\text{s}}$. This outstanding sensitivity is good enough for the detection of both teleseismic waves and near source seismic signals. Typical seismic signals require a high sensor stability for up to one hour of continuous data acquisition. This requirement is much reduced from the long-term stability necessity of an instrument for the measurement of Earth rotation variations. Of more importance is the short-term precision and mechanical rigidity of the laser beam path for stable operation. The instrument must be capable of accurately recording seismic rotations while keeping the scaling factor (the quotient in equation 1) constant. At the same time the whole system must be relocatable, cost effective and allow for a relatively simple installation. Given the fact that a ring laser is a highly sensitive optical interferometer, all these requirements are essentially contradicting design goals. For the data logging, a precise time stamping of the record is absolutely crucial for the desired application. A typical requirement for timing accuracy in seismology is to within 1 ms of UTC. As a consequence all data must be sampled using a stable reference and an accurate time such as the timescale represented by GPS.

2.1 GEOSensor Concept

In sect. 1 we have listed the requirements for a ring laser in seismology. The frequency band of interest covers about 5 orders of magnitude, while the corresponding sensitivity for the measurement of rotations should cover 14 orders of magnitude, the range between strong motions during a local earthquake on one side and the signals of an earthquake more than 10000 km away on the other side. However, if we exclude strong motion domain from the immediate measurement interest, we obtain a viable measurement range for a prototype sensor of approximately 10^{-12} rad/s $\Omega_s 10^{-4} \text{ rad/s}$ which still extends over 8 orders of magnitude.

The basic design of the GEOSensor is outlined in the block diagram of fig. 1. A synchronously generated dataset contains the precise timestamping from a GPS system, the instantaneous Sagnac frequency from the ring laser component, tiltmeter recordings in two directions about the normal vector of the ring laser plane and the measured velocities of a seismometer.

In order to operate the GEOSensor, more signals such as the ring laser beam intensity are required. However, such signals are used in a feedback system to set the operation range of the ring laser and therefore are not logged for further use.

2.2 The Ring Laser Component

In order to obtain a stable interferogram of the two laser beams the cavity length has to be kept constant to within a fraction of a wavelength. Therefore, usually ring laser bodies are made from Zerodur, a glass ceramic which

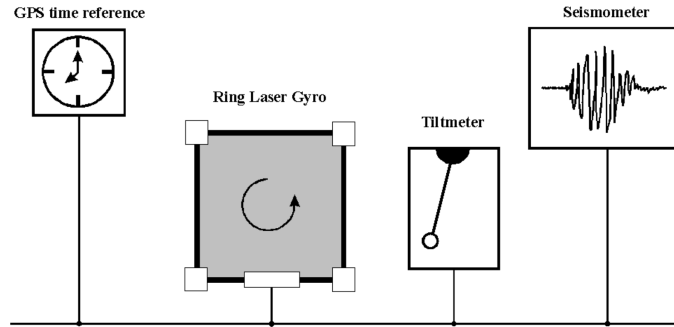


Fig. 1. Block diagram of the GEOsensor design.

exhibits a very small relative thermal expansion of $\alpha = 5 \cdot 10^{-8} \text{ 1/K}$. Since a ring laser for seismic applications requires an enclosed area of more than 1 m^2 , a monolithic ring construction would be both too expensive and not transportable.

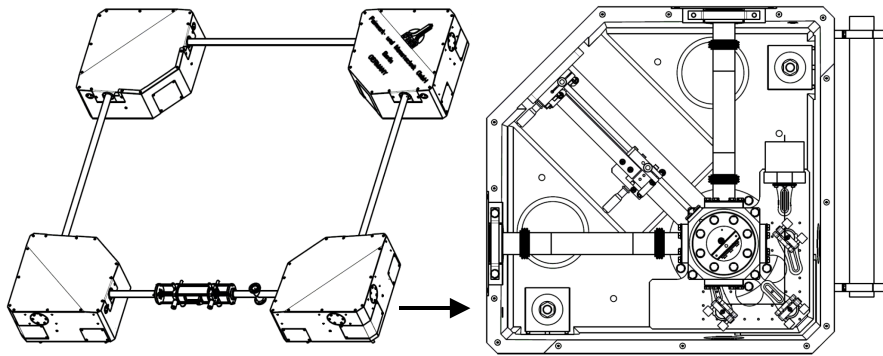


Fig. 2. Construction diagram of the GEOsensor ring laser.

Figure 2 gives an impression of the actually realized ring laser hardware. The laser cavity has the shape of a square. The 4 turning mirrors are each located in a solid corner box. As shown in the right side of the plot, a folded lever system allows the alignment of each mirror to be within ± 10 seconds of arc. This high level of alignment is required to ensure lasing from an optically stable cavity. The mirrors are located inside steel containers which in turn are connected together with stainless steel tubes, forming an evacuated enclosure for the laser beams. In the middle of one side the steel tubes are reduced to a small glass capillary of 4 mm in diameter and a length of 10 cm, which is required for gain medium excitation. When operated, the ring laser

cavity is first evacuated and then filled with a mixture of Helium and Neon reaching a total gas pressure of approximately 6 hPa. The left part of fig. 2 gives an impression of the instrumental layout. The following two important considerations are unique for the GEOsensor design.

- Since the ring laser is constructed from several components, it requires a stable concrete platform base at the location of deployment. Such a pad is simple to specify and can be prepared totally independently of the actual GEOsensor deployment.
- The actual area of the ring laser component is not predetermined by the design. The instrument can be built according to the available space at the host observatory. Different GEOsensor realizations may therefore have different size and consequently different instrumental resolution. The length of the current instrument is 1.6 m on a side, which provides an area of 2.56 m².

In order to operate the GEOsensor, the cavity must be evacuated, baked and filled with a Helium/Neon gas mixture. This procedure requires a turbo molecular pump system and a manifold with a supply of ⁴He, ²⁰Ne and ²²Ne. The pump system is not required during the operation of the GEOsensor but is necessary for the preparation of the instrument and once or twice during a year in order to change the laser gas. Laser excitation itself is achieved via a high frequency generator (Stedman, 1997), matched to a symmetrical high impedance antenna at the gain tube. A feedback loop maintains the level of intensity inside the ring laser and ensures monomode operation. When the ring laser is operated it detects the beat note caused by Earth rotation. The magnitude of this beat frequency is depending on $\sin(\Phi)$ with Φ the latitude of the ring laser location. Table 1 shows the value of the Earth's rate bias for a few locations of interest.

Table 1. Earth rotation bias for some GEOsensor locations

location	frequency [Hz]
Wettzell, Germany (49.145 N)	138
Pinon Flat, CA (33.6 N)	102
Tokyo (35.4 N), Japan	106
Cashmere (43.57 S), NZ	127

To date we have operated the GEOsensor at the first two locations. Since the Earth rotation acts like a rate bias on our ring laser measurements, any rotations caused by earthquakes will show up as an alternating frequency around the measured Earth rate.

2.3 Auxiliary Sensors

Ring lasers are rotation sensors that give very localized information on rotations. This is in contrast to an array of seismometers for example. To fully exploit the sensor potential and to investigate the properties of the GEOSensor instrumentation, other auxiliary data is measured along with the Sagnac frequency. The temperature at the monument of the ring laser installation provides informations on the scale factor variations due to the thermal expansion of the concrete foundation to which the ring laser hardware has been matched by design. Atmospheric pressure variations may also cause scale factor changes and are therefore measured too. For the purpose of studies on the general sensor behavior there is the option of logging the power of the high frequency generator and the beam power ratio. However this is not done routinely. The intensity of one laser beam is used to adjust the point of operation of the ring laser. This process is part of an automatic feedback loop arrangement but the data is currently not logged.

Apart from these direct ring laser related sensors we are recording variations in the orientation of the ring laser with respect to local \mathbf{g} as well as all three components of translational seismograms. The tiltmeter measurements are used to reduce the measured rotation rate from orientation effects that enter the Sagnac frequency via the inner product in equation 1. The importance of this effect is discussed in section 2.7 in more detail.

2.4 Logging System

The logging system has to satisfy demanding realtime conditions. This requires that the epoch of an observation can be timestamped to better than 1 ms with respect to UTC. The concept chosen for that purpose is outlined in fig. 3. The GPS time-frequency receiver provides both the time stamping and the data sampling frequency. The incoming PPS (pulse per second) signal with an accuracy of 30 ns rms relative to UTC, triggers the acquisition. The exact epoch of the trigger is also taken from the GPS receiver. The data sampling is based on a receiver reference frequency output, which has a relative accuracy of better than 10^{-12} (while locked to GPS). To satisfy the 1 ms accuracy requirement for the application, the reference frequency (e.g. 10 MHz) output is divided down to 1 kHz, which is the actual data acquisition rate. This frequency is used as an external clock instead of the build-in computer clock. This ensures that the data logging is always started at the full second and the data samples are equidistant and phase locked to the GPS receiver clock.

2.5 Deployment

After the development of the GEOSensor and including a test installation at the Fundamentalstation Wettzell, the instrument was shipped to the Scripps

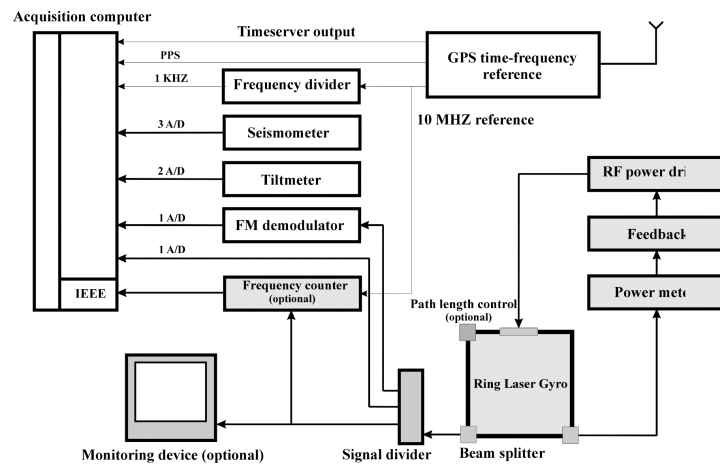


Fig. 3. Dataflow chart for the realtime logging in the GEOsensor

Institution of Oceanography in San Diego, California. In January 2005 the installation of the complete sensor took place at the seismological observatory Pinon Flat as shown in fig. 4. The observatory is located between the San Jacinto and the San Andreas faults.



Fig. 4. The ring laser vault at the Pinon Flat (CA) observatory and the GEOsensor installation in one of the chambers.

The goal of this installation is the measurement of a number of earthquakes at short distances from their epicenters. This will allow an extensive and systematic study of rotational motions with a particular emphasis on local and regional scales with source distances of up to 1000 km. From basic theoretical studies (Takeo and Ito, 1997) it became apparent that rotational motion information may contribute the most for local and regional earthquakes.

2.6 Sensor Performance and Verification

The validation of ring laser measurements as true rotational signals was an important item during the integration phase. For the assessment of the quality of the GEOsensor data it is necessary to distinguish true measured rotations from unknown sensor artefacts. Since there are two collocated ring lasers with identical orientation in the Cashmere Cavern in Christchurch, we used the simultaneous earthquake recording of both C-II and UG1 for the Fiji event on August 19, 2002. Figure 5 shows the Sagnac frequency as a function of time converted to rotation rate in nanoradians per second using equation 1 for the first 15 seconds of this earthquake.

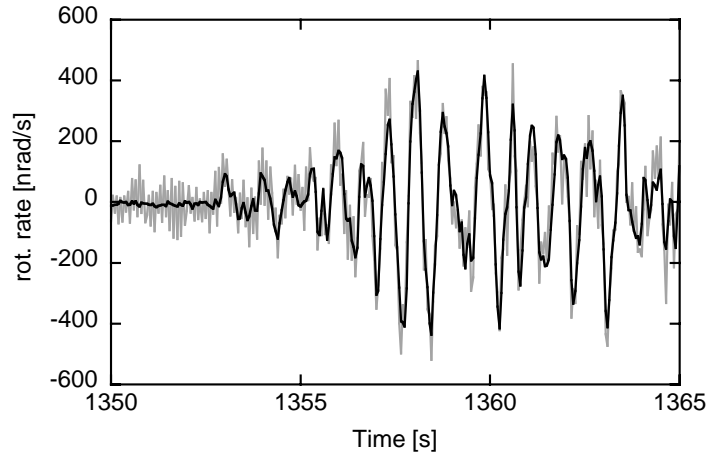


Fig. 5. Raw rotations obtained from an earthquake at Fiji (Aug. 19. 2002) with 2 collocated ring lasers C-II and UG1 located in the Cashmere Cavern near Christchurch (New Zealand)

Because ring lasers are purely optical sensors, they do not depend on mass inertia like ordinary seismometers. Therefore, there is no need for a restitution process of the measurement quantity. According to the ring laser equation the relationship between the obtained Sagnac frequency and the input rotation rate is linear over a wide dynamic range. This important property is reflected in fig. 5. The data from the small C-II ring laser is much more noisy than the data from the very large UG1, because there is almost a factor of 20 difference in the respective scale factors. Nevertheless one can see that both ring lasers measure the same effect, in phase as well as in amplitude. It has to be noted that apart from the unit conversion we are comparing raw data for this measurement.

2.7 Sensor Orientation

Equation 1 shows another very unique property of ring lasers. They measure absolute rotations and this includes also changes of the instrumental orientation as one can see from the inner product between the rotation axis and the instrumental normal vector. Ring lasers may be subject to rocking motions in the presence of S- and Rayleigh- waves one could argue. In order to identify such motions and to correct for this, the GEOSensor was equipped with a sensitive tiltmeter. Figure 6 shows an earthquake in Northern Algeria on May 21, 2003, which was measured at the G ring laser in Southern Germany approximately 1600 km away. The top part of the diagram shows the measured rotation rates from the ring laser, while the lower part of the diagram shows the corresponding contribution to the signal originating from variations of the ring laser orientation.

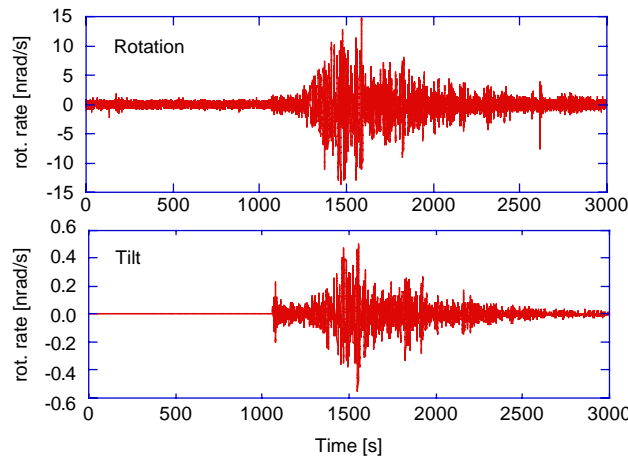


Fig. 6. Algerian earthquake real rotations and orientation induced variations of the Sagnac frequency expressed in the same units

This tilt equivalent rotation rate was computed by

$$\Omega_{tilt} = \Omega \cdot \sin(\Phi - T_{NS}), \quad (2)$$

where Ω is the actual rotation rate, Φ the latitude of the sensor and T_{NS} the North - South component of the locally measured tilt. The contribution of the East - West component is more than 2 orders of magnitude smaller, since it appears under a cosine function which is always very close to 1.

2.8 Detection Properties

Ring lasers provide optical interferograms where the external rate of rotation is proportional to the rate of change of the fringe pattern. This signal becomes

available as an audio-frequency at the output of a photomultiplier tube. In seismology it is important to detect the rate of change of this frequency at 50 ms intervals (20 Hz) very accurately. Since frequency counting techniques do not provide a sufficient resolution at such short averaging intervals, a frequency demodulation concept has been developed. A voltage controlled oscillator is phase locked to the Sagnac frequency of the ring laser, exploiting the fact that Earth rotation provides a constant rate bias in the absence of any seismically induced rotation signals. In the event of an earthquake one obtains the rate of change of the Sagnac frequency at the feedback line of the voltage controlled oscillator. This voltage can be digitized and averaged at the required 20 Hz rate or higher.

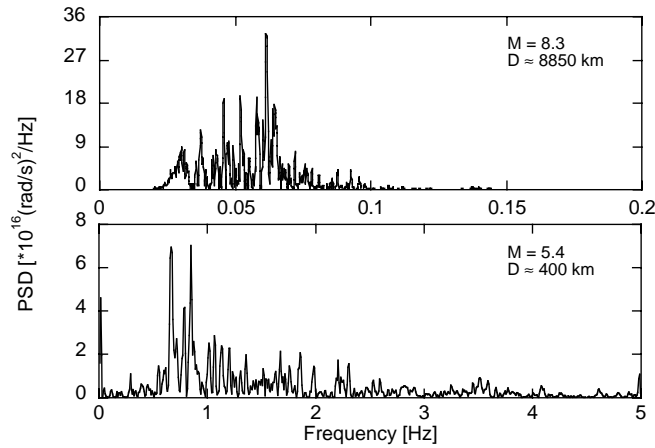


Fig. 7. Comparison of recorded rotation spectra from an teleseismic event (Hokkaido: Sept. 9, 2003) and a regional earthquake (France: Feb. 22, 2003). The much higher bandwidth of the rotational wave spectra requires data acquisition techniques such as the demodulator

To outline the importance of the frequency demodulation technique we compare two earthquakes with distinctly different properties. Figure 7 shows an example for a teleseismic event and an example from a much closer regional earthquake. While for the remote earthquake the spectral power density essentially drops off to zero above frequencies of 0.1 Hz, one can still see some signal signature up to about 4 Hz for the regional event. Frequencies with a rate of change above 2 Hz; however, are already outside the regime of reliable representation in phase and amplitude by conventional frequency counting and second order autoregression frequency analysis (McLeod et al., 2001(@)).

2.9 Sensor Artefacts

Large ring lasers are currently the most sensitive operational devices for the measurement of geophysically induced rotations. The GEOSensor combines the high sensitivity of these gyroscopes with a technical design that allows a relative simple deployment at an observatory with some basic infrastructure, such as a concrete pad in a basement of a building, electricity and internet connectivity. However, in the presence of even moderate temperature fluctuations, one has to accept sudden mode jumps in the laser cavity, since thermal expansion or compression changes the length of the ring laser cavity enough that a neighbouring longitudinal mode starts to have more laser gain than the currently supported one. Another side effect of these mode drifts is a slow change of mode pulling (Aronowitz, 1971) as the laser mode passes through the gain curve. For frequencies below 0.01 Hz this may result in some ambiguities for the interpretation and some post processing may be required to distinguish between seismically induced rotations and internal biases from the ring laser.

Figure 8 shows a sample dataset from the GEOSensor measured at the temporary installation on the Fundamentalstation Wettzell. The upper diagram shows a section of the measured rotations from the magnitude 7.4 Hokkaido earthquake from Sept. 5, 2004.

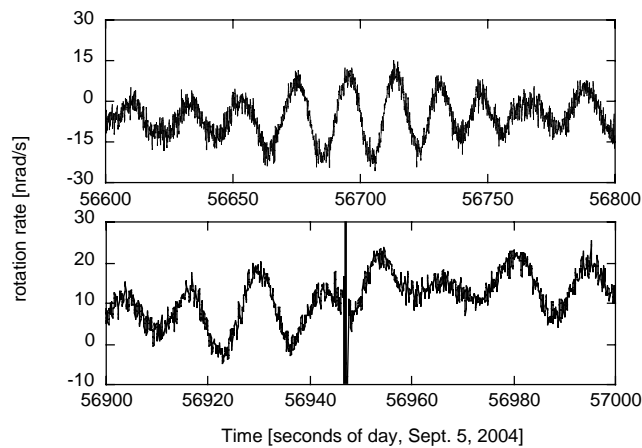


Fig. 8. Rotation measurements taken with the GEOSensor on Sept. 5, 2004. The top diagram shows obtained rotation rate, while the lower plot illustrates the effect of a mode jump in the data

In the lower diagram one can see the effect of a mode jump in the dataset. For about one second there is a gap in the data. This is the time it takes for the new mode to settle in and for the fringe pattern to become stable again.

For teleseismic events it is not difficult to interpolate the dataset and such a sensor behavior will not result in data loss. However for local earthquakes this may be different.

The effect of sensor drift is also apparent in fig. 8. One would expect the measured rotations to appear symmetrically about the rate bias of Earth rotation. This is not the case for the displayed dataset because of variations of the laser frequency pulling in the ring laser cavity. For earthquakes like the one shown here this artefact can be fully removed.

3 Data Analysis

3.1 Observations of rotations

In order to compare translations (measured by a standard seismometer) with the vertical component of the vector of rotation - which is what the G-ring is measuring - the horizontal components of seismic recordings were rotated into radial and transverse directions. Note that Rayleigh waves should not generate such a vertical rotation component, while Love waves are horizontally polarized hence generate rotations around a vertical axis only. To obtain transverse acceleration, the transverse velocity seismograms were differentiated with respect to time. Let us now assume a transversely polarized plane wave with displacement $\mathbf{u} = (0, u_y(t - \frac{x}{c}), 0)$, c being the horizontal phase velocity. The vector of rotation is thus given as $\frac{1}{2}\nabla \times \mathbf{u} = (0, 0, -\frac{1}{2c}\dot{\mathbf{u}}_y(t - \frac{x}{c}))$ with the corresponding z-component of rotation rate $\Omega_z(x, t) = -\frac{1}{2c}\ddot{\mathbf{u}}_y(t - \frac{x}{c})$. This implies that - under the given assumptions - at any time rotation rate and transverse acceleration are in phase and the amplitudes are related by $\ddot{\mathbf{u}}_y(x, t)/\Omega_z(x, t) = -2c$. In practice, the phase velocities can be estimated by dividing best-fitting waveforms in sliding a time-window of appropriate length along the seismic signal and rotation rate. Thus, under the plane-wave assumption both signals should be equal in phase and amplitude (McLeod et al., 1998; Pancha et al., 2000). This assumption is expected to hold for a considerable part of the observed ground motion due to the large epicentral distance compared to the considered wavelengths and source dimensions. This property is exploited here to verify the consistency of the observations. Close to the seismic source this assumption no longer holds and may form the basis for further constraining rupture processes (Takeo, 1998; Takeo and Ito, 1997).

A data example (rotation rate and transverse acceleration) of the M8.1 Tokachi-oki event, September 25, 2003, and a time-dependent normalized cross-correlation coefficient (maximum in a 30s sliding window) is given in fig. 9. The time window also contains an event (increase in cross-correlation at 3500 s) that was barely visible in the seismograms without correlating the two signals. When the waveform fit between rotation rate and transverse acceleration is sufficiently good (e.g., a normalized correlation coefficient > 0.95), we estimate phase velocities by dividing the peak amplitudes of both

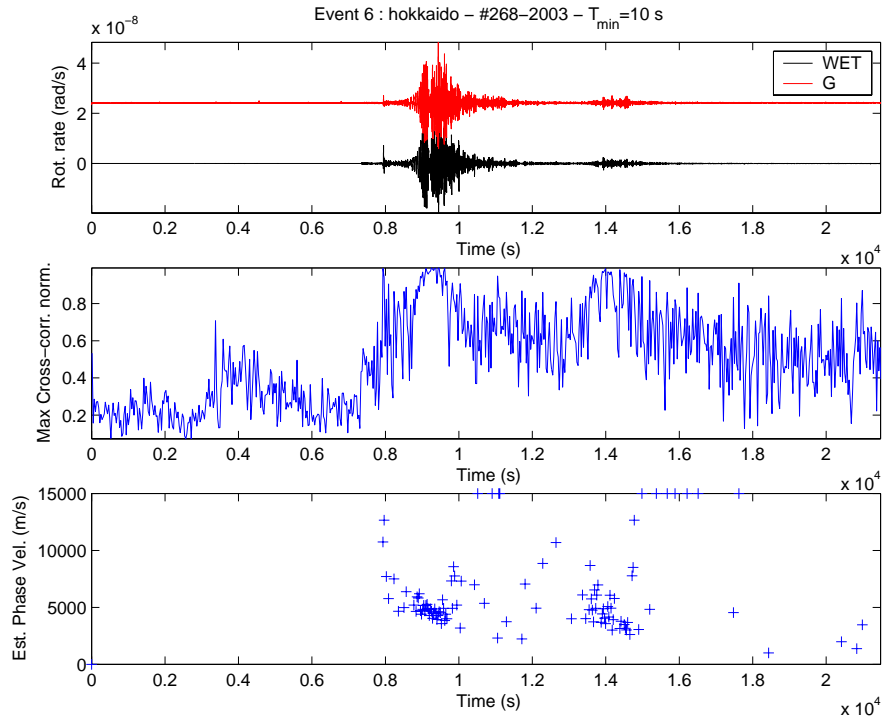


Fig. 9. Top: Observation of rotation rate (red) and transverse acceleration (black) after the M8.1 Tokachi-oki event, 29-9-03. Middle: The cross-correlation-coefficient in a 30 s sliding window. Note the increase in correlation during the main shock (>7500 s) and aftershock (>13800 s) to almost 1 (perfect match). Bottom: Estimates of horizontal phase velocities in time windows with good phase match (> 9500 s). Note the decreasing phase velocities in the Love wave train (e.g., 8000-10000 s, indicative of Love wave dispersion).

traces as explained above. These time dependent estimates of phase velocities are shown in fig. 9 (bottom). Despite the scattering the phase velocities in the time window containing the Love waves (9000-10000 s and around 14000 s for the aftershock) the estimates are in the right range of expected phase velocities and the negative slope of the velocities with time suggest that the expected dispersive behavior (earlier longer periods have higher phase velocities) can be observed in the data using this processing approach. The lack of correlation in the time windows excluding the Love waves may indicate that either the (body-) wave fronts are not planar or that the energy comes from out-of-plane directions through scattering. The consequence of non-planar waves on structural interpretation was studied by (Wielandt, 1993). To demonstrate that we obtain such a fit consistently we further show in fig. 10 on p. 17 the standard seismograms (blue) and a comparison between translations and observations

for another event out of a data base with now over 40 events with epicentral distances from 300-12000km.

3.2 Simulation of rotational motions in realistic Earth models

As there are basically next to no studies of rotational ground motions in the seismological literature several classic schemes to calculate synthetic seismograms have been extended to also output rotations. These are (1) the full space analytical solution of wave propagation due to a double couple point source e.g. (Aki and Richards, 2002) (with a surprising result at first sight: as expected, the rotation generated by the P wave-front is always zero - hence in particular in the far-field - yet the rotation derived from the far-field displacement alone is nonzero - as is obvious from the classical radiation pattern plot; one has to take all field terms into account. In other words, the usual separation between far-, intermediate-, near- displacement fields is not valid for rotations (Cochard et al., 2005)); (2) the Cartesian finite-difference algorithms with which we study near-source effects (Cochard and Igel, 2004); (3) the spherical finite-difference methods (Igel et al., 2002); and (4) the spectral-element code (Specfem) (Komatitisch and Tromp, 2002a,b). The latter algorithm was used to specifically model individual earthquakes using finite fault models (Igel et al., 2004, 2005b). The M8.1, Sep. 25, 2003, Tokachi-oki event was modelled with the Specfem algorithm (Igel et al., 2005a; Schuberth et al., 2004) using a 3D tomographic model, crustal model and a finite source model provided by Ji Chen (CalTech). The results of this modelling exercise is shown in fig. 11 on p. 18. The fit between observations and modelling for the shear-wave arrivals and the fundamental mode Love waves is excellent for both translations and rotations. The amplitude mismatch in the Love waves may be explained with the inaccurate finite source model leading to directivity effects that are not correctly modelled. However, it is important to note that the observed phase velocities match well with the modeled horizontal phase velocities (Igel et al., 2005a).

3.3 Long-period rotations

How much long-period information is contained in the ring laser recordings? In fig. 12 on p. 19 the transverse accelerations and rotations are again superimposed and filtered in narrow frequency bands to highlight the fit towards lower frequencies. This also allows us to directly estimate best-matching phase velocities in the Love-wave train and to see whether the expected dispersion relation is visible. Figure 12 on p. 19 demonstrates that the ring laser rotations are matching the transverse accelerations down to periods of 150 seconds (and possibly beyond). As expected the maximum amplitudes occur within the Love waves. By dividing the peak amplitudes of acceleration and rotation rate we estimate the phase velocities for narrow-bandwidth surface wave signals. As surface waves are dispersive as a consequence of the seismic velocity

structure with depth we expect increasing horizontal phase velocities with increasing dominant period. This is indeed what we observe at least in the band between periods of 20 seconds to 100 seconds. It is important to note that with the collocated recordings of rotations and translations one can estimate a quantity (phase velocity) that otherwise can only be determined with an array of seismometers or with collocated strainmeters (Mikumo and Aki, 1973). The results in fig. 12 on p. 19 are indeed promising. Even though this is work in progress the frequency-dependent amplitude ratio of rotations and translations suggests that a single-station measurement may allow estimates of Love-wave dispersion. These in turn would allow estimates of local 1D velocity models and - by combining several of them - eventually 3D tomography. However, whether the accuracy required for structural inversion is sufficient remains to be seen.

In summary, to the standard seismologist the current data base of rotations, array data, and collocated translations provides a realm of new opportunities. Even though the potential benefits to seismology, earthquake physics, and earthquake engineering still need to be further explored, the preliminary results indicate the many interesting new routes that can be taken.

Acknowledgement. This is publication no. GEOTECH-169 of the programme GEOTECHNOLOGIEN of BMBF and DFG, Grant 03F0325 A-D. The authors would like to thank Wolfgang Schlüter and Michael Wensauer from the Bundesamt für Kartographie und Geodäsie for their support of the project. We would also like to acknowledge the IQN Program by the German Academic Exchange Service and the Leibniz Computing Centre Munich for providing access to their supercomputers. We would like to thank Dr. Walter Zürn and Prof. R. Dunn for their constructive comments that improved the manuscript.

References

- Aki, K., Richards, P. G. (2002) Quantitative Seismology, 2nd Edition, University Science Books
- Aronowitz, F. (1971) The laser gyro. Laser applications, Vol. 1, edited by M. Ross, 133–200, Academic Press, New York
- Bouchon, M., and Aki, K. (1982) Strain, tilt and rotation associated with strong ground motion in the vicinity of earthquake faults. Bull. Seismol. Soc. Amer., 72:1717–1738
- Cochard, A., Igel, H. (2003) What can rotational measurements teach us about earthquake rupture histories? Eos Trans. AGU, 84(46), Fall Meet. Suppl., Abstract S42D–0200
- Cochard, A., Igel, H. (2004) What can rotational measurements teach us about earthquake rupture histories? Geophysical Research Abstracts (EGU Meeting), 6, 06359
- Cochard, A., Igel, H., Flaws, A., Schuberth, B., Wassermann, J., Suryanto, W. (2005) Rotational motions in seismology, in preparation, to be published in “Earthquake

- source asymmetry, structural media and rotation effects” eds. Teisseyre et al., Springer Verlag
- Igel, H., Nissen-Meyer, T., Jahnke, G. (2002) Wave propagation in 3-D spherical section: effects of subduction zones, *Phys. Earth. Planet. Int.*, 132:219–234
- Igel, H., Flaws, A., Velikoseltsev, A., Cochard, A., Schreiber, K. U. (2004) Comparison of rotational and translational motions induced by distant large earthquakes, *Geophysical Research Abstracts (EGU Meeting)*, 6, 06487
- Igel, H., Schreiber, K. U., Flaws, A., Schuberth, B., Velikoseltsev, A. Cochard, A. (2005a) Rotational motions induced by the M8.1 Tokachi-oki earthquake, September 25, 2003, *Geophys. Res. Lett.*, VOL. 32, L08309, doi:10.1029/2004GL022336
- Igel, H., Cochard, A., Schuberth, B., Flaws, A. Velikoseltsev, A., Schreiber K. U. (2005b) Rotational ground motions: a new observable for seismology? *Geophysical Research Abstracts (EGU Meeting)*, 7
- Komatitsch, D., Tromp, J. (2002a) Spectral-element simulations of global seismic wave propagation, Part I: Validation, *Geophys. J. Int.*, 149:390–412
- Komatitsch, D., Tromp, J. (2002b) Spectral-element simulations of global seismic wave propagation, Part II: 3-D models, oceans, rotation, and gravity, *Geophys. J. Int.*, 150:303–318
- McLeod, D. P., Stedman, G. E., Webb, T. H., Schreiber K. U. (1998) Comparison of standard and ring laser rotational seismograms, *Bull. Seism. Soc. Amer.*, 88:1495–1503
- McLeod, D. P., King, B. T., Stedman, G. E., Schreiber, K. U., and Webb T. H. (2001) Autoregressive analysis for the detection of earthquakes with a ring laser gyroscope; *Fluctuations and Noise Letters*, Vol. 1, No. 1:R41–R50
- Mikumo, T., Aki, K. (1973) Determination of local phase velocity by intercomparison of seismograms from strain and pendulum instruments, *J. Geophys. Res.*, 69, 721–731
- Pancha, A., Webb, T.H., Stedman, G. E., McLeod, D.P., and Schreiber, U. (2000) Ring laser detection of rotations from teleseismic waves. *Geophys. Res. Lett.*, 27:3553–3556
- Schreiber, U., Schneider, M., Rowe, C.H., Stedman, G. E., and Schlüter, W., (2001) Aspects of Ring Lasers as Local Earth Rotation Sensors. *Surveys in Geophysics*, Vol. 22, Nos. 5-6:603–611
- Schreiber, U., Velikoseltsev, A., Stedman, G. E., Hurst, R. B., Klügel, T. (2004) Large Ring Laser Gyros as High Resolution Sensors for Applications in Geoscience. *Proceedings of the 11th International Conference on Integrated Navigation Systems*, St. Petersburg, 326–331
- Schuberth, B., Igel, H., Wassermann, J., Cochard, A., Schreiber, K. U. (2004) Rotational Motions from Teleseismic Events - Modelling and Observations, *Eos Trans. AGU, Fall Meet. Suppl. Abstract S42D–0200*
- Stedman, G. E., Li, Z., Bilger, H. R. (1995) Sideband analysis and seismic detection in large ring lasers. *Appl. Opt.*, 34:7390–7396
- Stedman, G. E. (1997) Ring laser tests of fundamental physics and geophysics. *Rep. Progr. Phys.* 60:615–688
- Takeo, M., Ito, H. M. (1997) What can be learned from rotational motions excited by earthquakes? *Geophys. J. Int.*, 129:319–329
- Takeo, M. (1998) Ground rotational motions recorded in near-source region of earthquakes, *Geophys. Res. Lett.*, 25:789–792

Trifunac, M. D., Todorovska, M. I. (2001) A note on the usable dynamic range of accelerographs recording translation, *Soil Dyn. Earth. Eng.*, 21(4):275-286
 Wielandt, E. (1993) Propagation and structural interpretation of non-plane waves, *Geophys. J. Int.*, 113, 45-53

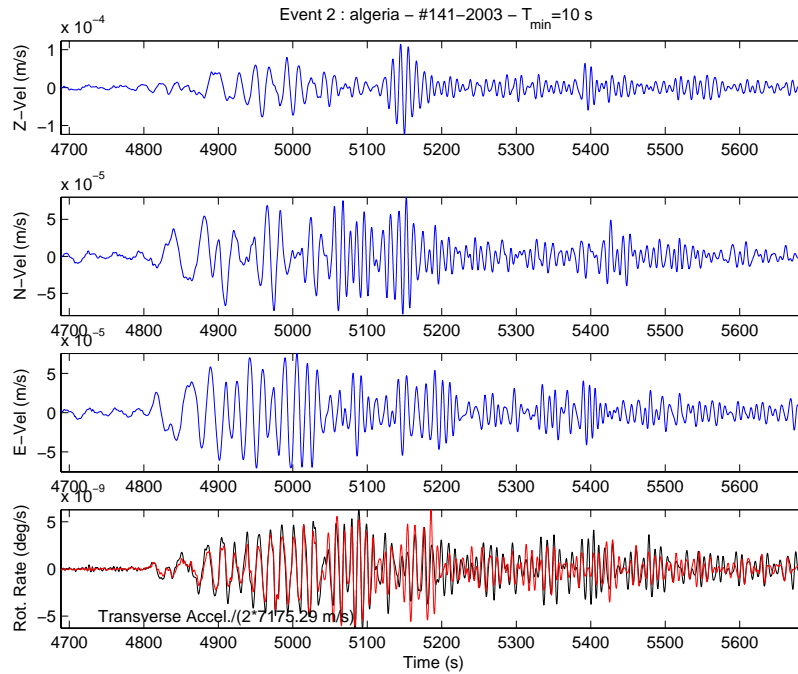


Fig. 10. Three components of translations (blue) and comparisons of transverse acceleration (black) and rotation rate (red) for one example in the event data base (superimposed traces at the bottom). Note the consistent match for most of the seismogram except towards the end where scattering may lead to phases arriving from out-of-plane directions. Conversion phase velocities are given in the lower left corner.

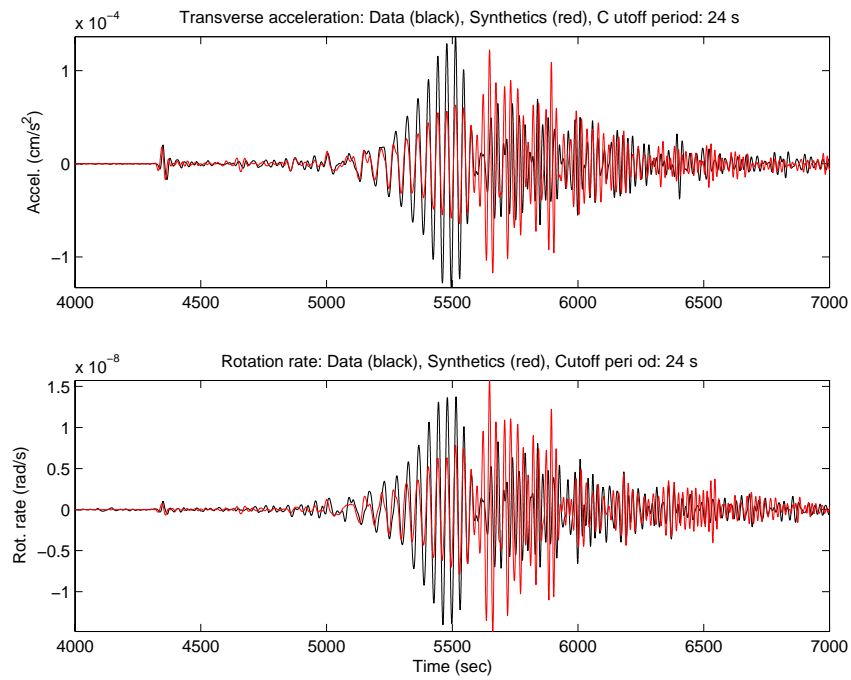


Fig. 11. Modelling of translational and rotational ground motions of the M8.1 Tokachi-oki event, September 25, 2003. Top: Observed (black) and modeled (red) transverse acceleration. Bottom: Observed (black) and modeled (red) rotation rate. All traces are shown with absolute amplitude. Note the excellent fit in waveform and amplitude of the direct S-wave (first onset) and the phase match of the fundamental mode Love waves. After 5500 seconds, not unexpectedly, the match is far from excellent, caused by the arrival of multipathing, scattered and/or non-plane waves.

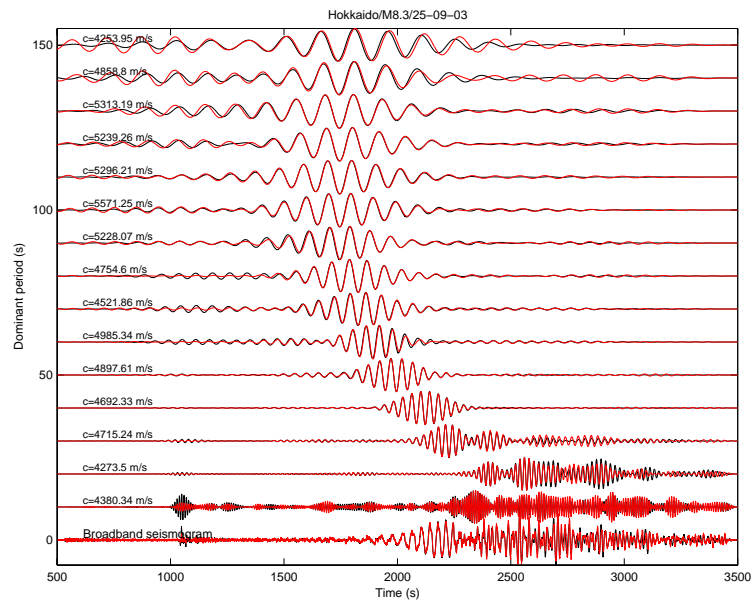


Fig. 12. Frequency dependent comparison of rotations (red) and accelerations (black). The vertical axis is central period of a very narrow band-pass filter. Note the excellent match at periods down to 150 s. Note also the general increase in best-matching phase velocities as expected from theoretical Love-wave dispersion.